Available online at www.sciencedirect.com
SCIENCE DIRECT®
Engineering Fracture Mechanics 72 (2005) 73–89
Engineering Fracture Mechanics
www.elsevier.com/locate/engfracmech

A hybrid experimental–numerical investigation of dynamic shear fracture

D. Rittel *

Faculty of Mechanical Engineering, Israel Institute of Technology, Technion City, 32000 Haifa, Israel

Received 24 July 2003; received in revised form 10 November 2003; accepted 22 January 2004

Abstract

Dynamic shear fracture is investigated by a hybrid experimental–numerical approach. The numerical simulations rely on LEFM assumptions and crack-tip stationarity. Violation of these assumptions is related to fracture or adiabatic shear banding and can be used to identify these events in a typical experiment. Firstly, the reliability of numerical model is verified by comparing our results with the analytical results of Lee and Freund [J. Appl. Mech. 57 (1990) 104]. Then a numerical simulation of Guduru et al.'s experiments is compared with their results to assess the onset of adiabatic shear banding in terms of a critical K_{II} value. Finally, dynamic shear experimental results are reported and analyzed using this approach for commercial PMMA and Maraging 250 steel specimens. In these experiments, the stress intensity factors are determined from miniature strain gauge measurements. A very good agreement is obtained between the present and previous values of K_{II}. The numerical exercises and the experimental results validate the use of hybrid experimental–numerical techniques for the identification of the onset of fracture, with a potential application to large-scale testing.

Keywords: Dynamic shear; Failure mode transition; Strain gauges; Hybrid experimental–numerical approach

1. Introduction

Dynamic mode II loading and subsequent fracture is more frequently encountered in the geophysical context than in engineering mechanics, as opposed to mode I. Yet, one cannot rule out situations in which a noticeable shear component is applied or develops at the tip of a crack. Therefore, this problem has raised much interest in the engineering community, essentially following the original work of Kalthoff et al. [9] who reported a failure mode transition related to the application of a dominant mode II condition at the tip of a dynamically loaded crack. Analytical work by Lee and Freund [12] provided a solution for the crack-tip fields for short times, such as to exclude wave reflections. This solution shows the potential development of a negative mode I component, as a result of crack/notch closure

* Tel.: +972-4829-3261; fax: +972-4832-4533.
E-mail address: merittel@tx.technion.ac.il (D. Rittel).
URL: http://www.technion.ac.il/~merittel.

0013-7944/$ - see front matter © 2004 Published by Elsevier Ltd.
doi:10.1016/j.engfracmech.2004.01.013

effects. In parallel, experimental and numerical results have been published, which describe the crack-tip fields for longer time durations [14,15]. Experimental work has concentrated on metallic materials (essentially Maraging steel, steel alloys and Ti alloys [22,24,25]), and the main experimental techniques used are based on optical methods, such as caustics [9] or CGS (coherent gradient sensing) [14,15]. In a relatively recent work, Ravi-Chandar [16] reported a similar failure mode transition in commercial polycarbonate, thus extending the concept of failure mode transition to a broad class of materials capable of sustaining crack-tip plasticity. The failure mode transition is related to the high strain-rate thermomechanical coupling which manifests itself as a noticeable elevation of the crack-tip temperature (see e.g. [19,24,25]). A vast part of these studies focused on running cracks, while others have emphasized initiation aspects of the dynamic failure process, including adiabatic shear band formation. In several of these works, the crack-tip stress intensity factors (SIF) were measured using optical methods, and it has been suggested that a critical value of the mode II component may trigger the failure mode transition [14,15,20,22].

Transient stress intensity factor characterization requires sophisticated equipment, to generate and record the selected optical pattern at the tip of a crack with a high sampling frequency, of the order of 1 million frames per second. On the other hand, the use of strain gauges in experimental fracture mechanics is well-documented [7], and a strain gauge setup has been proposed to determine directly the stress intensity factors [5]. Strain gauges have also been extensively used to investigate interfacial fracture problems (see e.g. [11,17]). In parallel, hybrid experimental–numerical methods have long been used to gather data that is not directly accessible experimentally [10]. Usually, an accurate numerical model is built to which the enforced initial and boundary conditions are those of a typical experiment. This approach was used by Bui et al. [4] to determine dynamic stress intensity factors. However, the hybrid experimental–numerical approach may have additional applications, such as assessing the range of validity of certain assumptions. For example, Maigre and Rittel [13] used the reciprocity theorem to assess the onset of dynamic crack propagation. The lack of similarity between the evolutions of the dynamic stress intensity factors calculated separately, using applied loads and displacements, was interpreted as an indication that the crack was no longer stationary, i.e. the onset of fracture. An additional example of a computational–experimental work can be found in Weisbrod and Rittel [23]. These authors investigated dynamic mode I fracture using small beam specimens. They compared experimental and calculated stress intensity factor based on a simple one-parameter description of the crack-tip fields. The comparisons showed an excellent agreement between the simulation and the experiment until the onset of fracture, determined using a single-wire fracture gauge. However, quite surprisingly, dynamic mode II characterization based on strain gauges has not been widely reported to the best of the author's knowledge.

Consequently, the present paper reports new results on the characterization of the dynamic crack-tip fields obtained using a combination of a simple strain gauge experimental setup coupled to finite element calculations. Numerical simulations are used as a tool to assess the onset of adiabatic shear band formation in terms of stress intensity factors. The present results compare quite well with those obtained using optical methods, so that the concepts shown here can serve as a basis for future large scale experiments.

The paper is organized as follows: firstly, the relevant fracture mechanics background, assumptions and numerical solution tools are presented. The second section describes the experimental setup and data processing techniques. Next, typical numerical and experimental results are presented for two characteristic materials: commercial polymethylmethacrylate (PMMA) and Maraging 250 steel in the aged condition. The next section discusses the results by establishing a comparison with previously reported results, as well as the implications of the present work to dynamic failure mode transition.

2. Theoretical background

2.1. Stationary crack subjected to transient loading—analytical

The crack-tip fields ahead of a stationary crack (thus excluding all propagation issue) can be expressed, as their static counterpart, in terms of the stress intensity factors. For transient loading, the stress intensity factor(s) vary with time [6], and one of the goals of the reported experiments is the determination of this variation. In this paper, we will confine ourselves to a single parameter description of the crack-tip fields, based on the SIF, excluding for the sake of simplicity the higher order terms that arise from the finiteness of the specimen. Generically, the stress (σ) and strain fields (ε) are written as

$$\begin{aligned}\sigma_{ij}(t) &= \frac{K(t)}{\sqrt{r}} f_{ij}(\theta) \\ \varepsilon_{ij}(t) &= \frac{K(t)}{\sqrt{r}} g_{ij}(\theta)\end{aligned} \tag{1}$$

In this expression, f_{ij}, g_{ij} and K depend on the loading mode(s). An analytical solution for a dynamically loaded crack, such as in Kalthoff's experiments [9], is given by Lee and Freund [12]. The solution shows that a dominant mode II component develops at the crack-tip, but an additional negative mode I component is also present, which tends to close the crack or notch. In a previous paper, Rittel and Levin [20] suggested that the introduction of a fatigue precrack would eliminate, or at least significantly reduce the interpenetration of the crack flanks. Denoting by $K_{\mathrm{I}}(t)$ and $K_{\mathrm{II}}(t)$ the two dynamic stress intensity factors, the strains at any point located at (r, θ) can be expressed in a cartesian coordinate system (Fig. 1) by

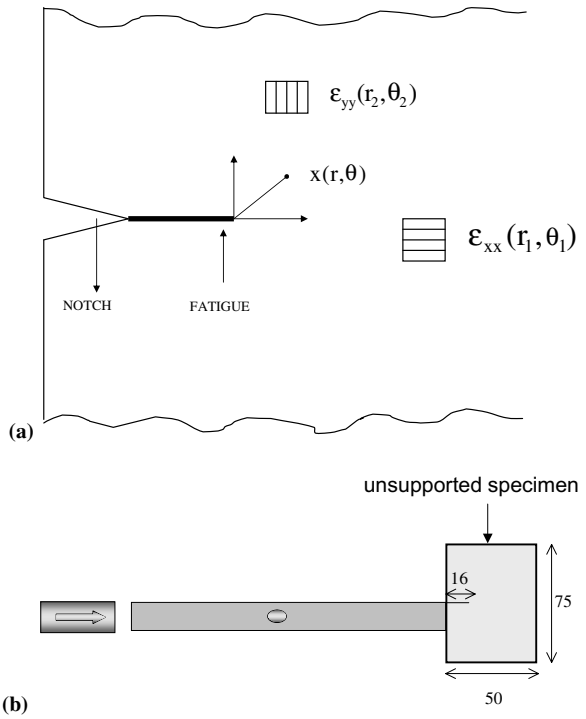

Fig. 1. (a) Strain gauge positions and coordinate system. (b) One-point impact experimental setup. All dimensions are in mm.

$$\begin{aligned}\varepsilon_{xx}(t) &= \frac{1}{E}\left[\frac{K_{\mathrm{I}}(t)}{\sqrt{2\pi r}}\cos\left(\frac{\theta}{2}\right)\left[(1-v)-(1+v)\sin\left(\frac{\theta}{2}\right)\sin\left(\frac{3\theta}{2}\right)\right]\right.\\ &\quad\left.-\frac{K_{\mathrm{II}}(t)}{\sqrt{2\pi r}}\sin\left(\frac{\theta}{2}\right)\left[2+(1+v)\cos\left(\frac{\theta}{2}\right)\cos\left(\frac{3\theta}{2}\right)\right]\right]\\ \varepsilon_{yy}(t) &= \frac{1}{E}\left[\frac{K_{\mathrm{I}}(t)}{\sqrt{2\pi r}}\cos\left(\frac{\theta}{2}\right)\left[(1-v)+(1+v)\sin\left(\frac{\theta}{2}\right)\sin\left(\frac{3\theta}{2}\right)\right]\right.\\ &\quad\left.+\frac{K_{\mathrm{II}}(t)}{\sqrt{2\pi r}}\sin\left(\frac{\theta}{2}\right)\left[2v+(1+v)\cos\left(\frac{\theta}{2}\right)\cos\left(\frac{3\theta}{2}\right)\right]\right]\end{aligned} \tag{2}$$

where E and v are Young's modulus and Poisson's ratio, respectively. Eq. (2) shows that two independent strain measurements are all that is needed to simultaneously determine $K_{\mathrm{I}}(t)$ and $K_{\mathrm{II}}(t)$. The measurements reported in this work will make use of this fact (see also [7]).

2.2. Stationary crack subjected to transient loading—numerical

A two-dimensional, dynamic analysis of the plate containing a *stationary crack* was carried out, using ANSYS [1] commercial finite element package. We assumed a *linear elastic* material behavior. The equation of motion for the cracked specimen is

$$\nabla \cdot \sigma = \rho \ddot{u} \tag{3}$$

where σ is the stress tensor, $\ddot{u}$ represents the displacement vector (superposed dots indicate time derivatives) and ρ is the material's density. The specimen lays unsupported and is initially at rest: $u(t=0)=0$; $\dot{u}(t=0)=0$; $\ddot{u}(t=0)=0$. The load $P(t)$ is applied to the part of the specimen which is contact with the input loading bar (Fig. 1 and Section 3).

The specimen was discretized into quadrilateral 8-node finite elements (PLANE 82). A state of plane stress was selected to simulate readings obtained on the surface of the specimen. The applied load was modeled as a pressure applied to the structure. This parameter could either be determined experimentally (for a subsequent hybrid experimental–numerical approach), or arbitrarily selected (for numerical experiment). Several load cases were investigated, including very short impulse and stepped load, as detailed in the following sections. The equation of motion was solved, using Newmark time integration scheme [3].

The crack-tip was modeled with quarter-point singular triangular elements [2]. The crack is actually a fatigue crack, susceptible of undergoing both contact and frictional stresses over its flanks, as a consequence of the (negative) mode I and mode II components respectively. Consequently, contact and frictional conditions were included in the model. Friction was assumed to obey Coulomb's law, with an assumed coefficient of friction of $\mu = 0.4$, as in our previous work [20]. Contact modeling, in its simplest form, includes the definition of a contact (E_{N}) and tangential stiffness (E_{T}). Two cases were modeled: a "hard" contact with $E_{\mathrm{N}} = Y$ and $E_{\mathrm{T}} = 0.1Y$ respectively ($Y =$ Young's modulus), and a "soft" contact for which $E_{\mathrm{N}} = 0.1Y$ and $E_{\mathrm{T}} = 0.1Y$ respectively. Mode I and mode II SIF's were determined from the displacements of two selected keypoints located at $r = 1$ mm and $\theta = \pi$ before the crack-tip, according to

$$K_{\mathrm{I,II}} = 4Eu_{y,x}\sqrt{\frac{2\pi}{r}} \tag{4}$$

where u is the x or y component of the displacement, and E is Young's modulus. While this method of determination of the SIF's is by no means the most accurate, it is probably the simplest and fastest for the present calculations involving many load steps.

3. Experimental

The specimens are rectangular plates (75 mm × 50 mm × 12.5 mm). A 12.5 mm notch was machined at mid-height of the specimen, and a fatigue precrack of variable length (typically 3 mm) was subsequently grown from the notch. Two materials were used in this study:

- Maraging 250 steel, with $E = 190$ GPa, $\nu = 0.3$, and $\rho = 7800$ kg/m^3;
- Commercial polymethylmethacrylate (PMMA), with $E = 3.5$ GPa, $\nu = 0.40$, and $\rho = 1180$ kg/m^3.

Two 0.2 mm strain gauges (KFG-020120-C1-11) were cemented in the vicinity of the crack-tip, at variable radii and angles, as detailed in the sequel. Each strain gauge formed one arm of a Wheatstone bridge. The gauge recorded a strain component, $\varepsilon_{xx}(t)$ and $\varepsilon_{yy}(t)$, to be processed using Eq. (2). Strain gauge signals were recorded differentially on a Nicolet 490 oscilloscope, with a sampling frequency of 2 MHz. Specimen loading was achieved in the one-point impact configuration (see e.g. [7]), in which the unsupported specimen is in contact with an instrumented (Hopkinson) bar, against which a projectile is fired with a air gun. The specimen is loaded through the bar until it takes off freely. The duration of loading is dictated by the specimen dimensions. Fracture occurs during the loading phase [21]. The bar signals (input pulse) were not recorded in these tests, as they were not needed for subsequent data processing. A single wire fracture gauge (MM-CD-02-15A) was cemented on the opposite side of the specimen to signal crack propagation. The experiments showed that this gauge did not provide reliable information, when cracking occurred by shear banding (steel) tunneling underneath the gauge without fracturing it. In other cases (PMMA), multiple fracture occurred so that the gauge information was useless. Consequently, the onset of fracture or shear band formation was not recorded in the present experiments. Upon completion of the experiment, the recovered specimen was examined to assess crack extension (steel) or shattering (PMMA).

4. Results

4.1. Numerical results

The forthcoming numerical results are aimed at establishing a comparison between our numerical simulations and previously reported results. This is a preliminary stage towards processing of the experimental results reported later.

4.1.1. Lee and Freund's [12] problem

These authors determined analytically the dynamic stress intensity factors of a cracked plate subjected to a step load. Their numerical results are found in Figs. 15 and 16 of [8]. The analytical and numerical solutions showed an excellent agreement for the mode II component, but these solutions diverged for the mode I component after a short normalized time of 1.4. The specimen geometry and boundary conditions are identical to those of our experiments, and the selected material is Maraging 250 steel. To allow for comparison, we assumed step loading, for which the applied pressure reaches unit value within 2 μs and is then held for another 40 μs. Fig. 2 shows the various crack opening displacements corresponding to two contact cases, "hard" and "soft". These results are not normalized in purpose. As expected, the mode II component is dominant. The evolution of the mode I component is strongly dictated by the selection of the contact parameters of the problem. When crack closure is allowed through a lower normal stiffness, a noticeable negative mode I component develops, as in [12].

Therefore, the "soft" case can be compared with the above mentioned results. Lee and Freund's [12] results are normalized according to

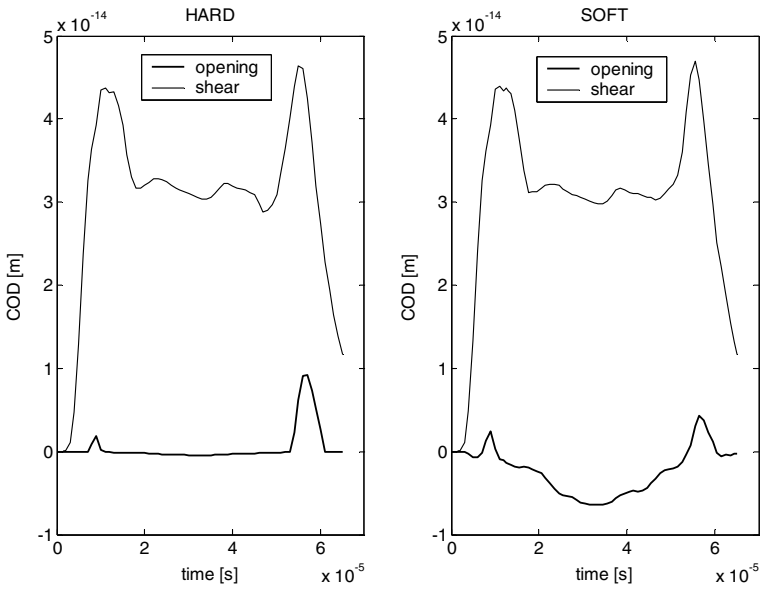

Fig. 2. Numerical simulation of Lee and Freund's results [12]. Crack-opening displacements for two different contact configurations. Note the dominant mode II. For the "soft" configuration, a noticeable negative mode I component develops.

$$t_n = \frac{c_d^{pl-\sigma} t}{l} \quad \text{and} \quad K_n = \sqrt{\frac{l}{\pi}} \frac{Ev}{2c_d^{pl-\sigma}} \tag{5}$$

where $c_d^{pl-\sigma} = 4690$ m/s is the plane stress dilatational wave speed, $l = 16.5$ mm is the crack length, t stands for time and v is the impact velocity. To allow for comparison with the present results, Eq. (5) will be used for the non-dimensional time, but the non-dimensional SIF will be divided by its absolute maximal value over the reported time interval. This additional normalization cancels the influence of the impact velocity that is not a boundary condition in our simulations. Fig. 3 shows this comparison. An excellent agreement is noted for the mode II component over the whole interval of time. For the mode I component, the agreement is limited to a shorter normalized time duration of the order of 1. These results are identical in essence to those reported by Lee and Freund [12]. As mentioned previously, the determination of the negative mode I depends strongly on the assumptions made for the contact between the crack flanks.

4.1.2. Guduru et al.'s [8] results

Guduru et al. [8] performed side-impact experiments, on a clamped fatigue precracked specimen. The specimen dimensions, material (Maraging C300 steel), and boundary conditions are detailed in their paper. These authors measured the SIF's using the coherent gradient sensing optical method. Here a 50 mm diameter 127 mm long projectile was used. For this relatively short projectile, experience shows that the resulting impact pulse is close to a gaussian or half cosine curve, whose duration is of the order of 50 μs. The crack length was 27.4 mm. Due to the presence of a fatigue crack, a "hard" contact configuration was assumed. The calculated and (averaged) reported SIF's are shown in Fig. 4, in non-dimensional form and suitable normalization as above-mentioned. An overall degree of similarity is noticeable between the simulation and the experiment. Closer examination reveals a high degree of similarity for short times up to $t \approx 3$ (K_I) and $t \approx 7$ (K_{II}), beyond which the calculation and simulation diverge increasingly. Guduru et al. [8] reported values of $K_{IIc} = 125$–190 MPa $\sqrt{m}$ for adiabatic shear band formation in the investigated range

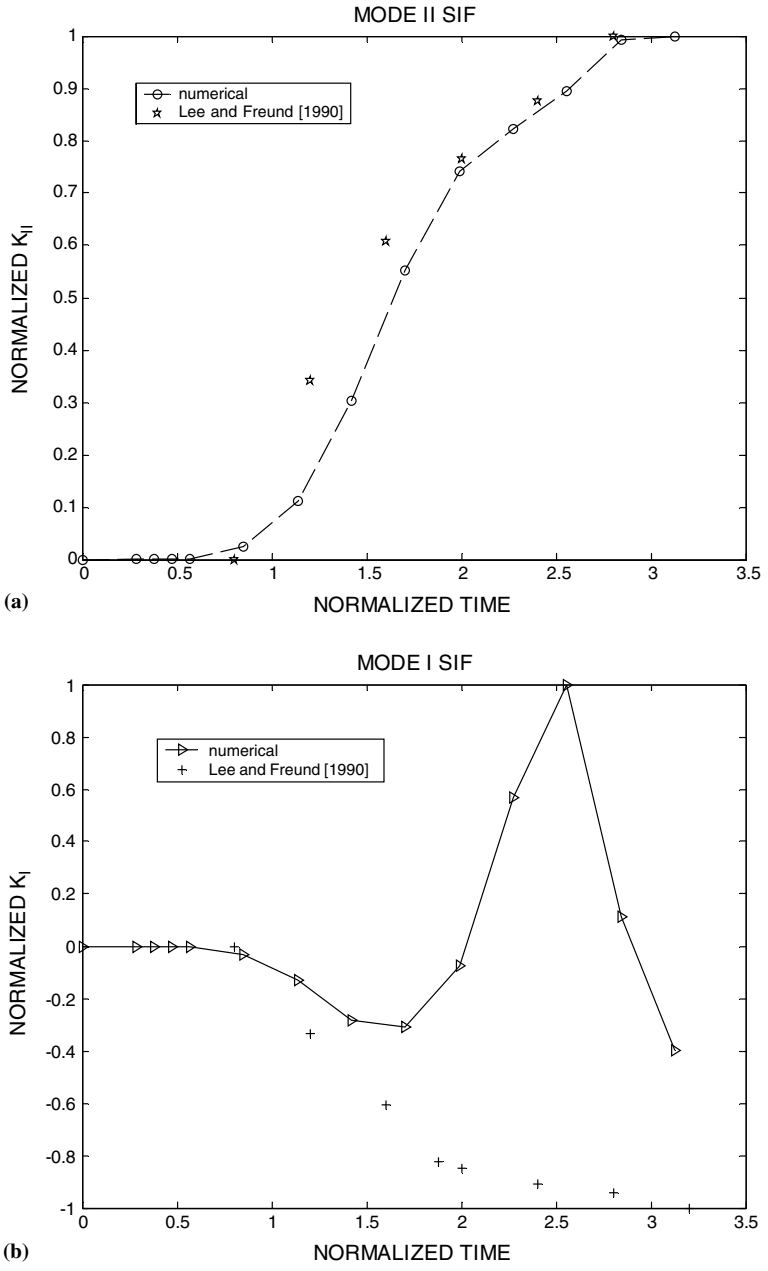

Fig. 3. Calculated stress intensity factors vs. Lee and Freund's results [12]: (a) mode II and (b) mode I.

of impact velocities 25–40 m/s (their Figs. 20 and 21). The corresponding normalizing SIF (Eq. (5)) is $K_n = 47$–76 MPa $\sqrt{\text{m}}$. Therefore, the critical ratio at shear band initiation is $\frac{K_{\text{IIc}}}{K_n} = 2.66$–$2.50$. This ratio can now be compared with the dimensional results published in their Fig. 14, which pertains to slightly smaller velocities in the range 15.5–23 m/s. For this range of velocities, a ratio of $\frac{K_{\text{IIc}}}{K_n} \approx 2.66$, corresponding to $K_{\text{IIc}} \approx 125$ MPa $\sqrt{\text{m}}$, is reached at $t_n \approx 3$. Fig. 4 shows that this is indeed the time at which the numerical

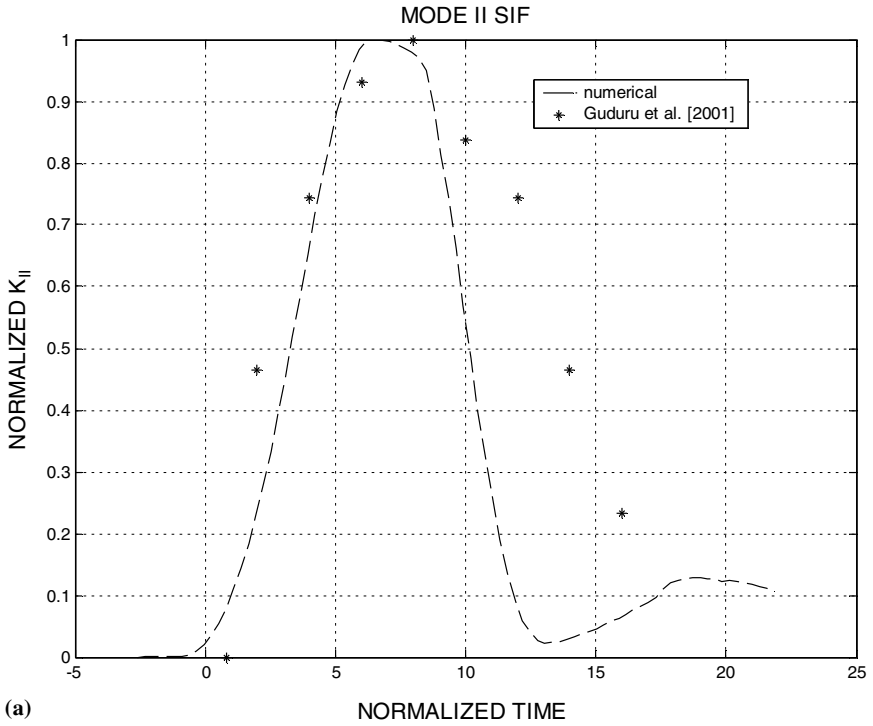

Fig. 4. Calculated stress intensity factors vs. Guduru et al.'s results [8]: (a) mode II and (b) mode I.

and actual experimental results diverge for the mode I component. However, divergence is observed at $t_n \approx 7$ for the mode II component, at which Guduru et al.'s [8] Fig. 14 yields a ratio $\frac{K_{II}}{K_n} \approx 4$. Here, the critical value for shear band formation becomes $K_{IIc} \approx 196$ MPa $\sqrt{\text{m}}$. From the mode I results, there is an excellent agreement with the observed time at which the numerically and the experimentally determined SIF values start to diverge. The degree of agreement is slightly inferior, for the mode II component. Yet, the adequacy between numerical and experimental results is overall quite satisfactory, given the experimental uncertainties and the numerical adjustable contact and stiffness parameters. As mentioned previously, the divergence is caused by the fact that the numerical simulation does not account for adiabatic shear band formation or crack propagation whatsoever, and is therefore reliable only until the onset of these failure phenomena.

Therefore, beyond the mere exercise of comparing numerical simulations to experiments, this comparison reveals that the numerical simulation can be used to some extent as a means to determine the onset of cracking or shear band formation, as will be further emphasized in the next section.

4.2. Experimental results

4.2.1. Polymethylmethacrylate specimen

The specimen was fatigue precracked to reach an overall initial crack length of 16 mm. Strain gauges were cemented at $r_1 = 3.24$ mm—$\theta_1 = 3°$ (parallel), and $r_2 = 3.25$ mm—$\theta_2 = -55°$ (perpendicular) respectively. As shown in Fig. 5, the specimen fractured by developing three almost simultaneous cracks. The strain gauge recordings are shown in Fig. 6(a), in which time has been normalized according to Eq. (5), and the strain values have been normalized by dividing the strain by the maximum absolute value of the two readings. The two strains signals grow initially together until $t \approx 1.5$, at which the parallel strain drops rapidly to zero. For the numerical calculations, a "hard" contact configuration was assumed, but this time

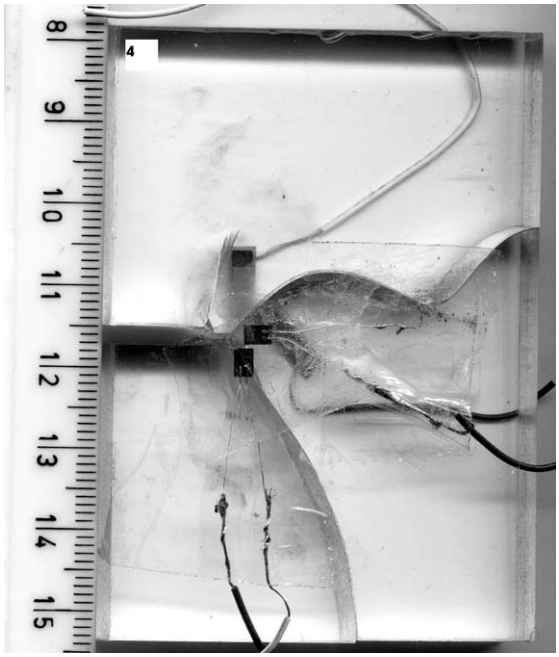

Fig. 5. A typical PMMA specimen after impact. Three simultaneous cracks originate from the fatigue crack-tip.

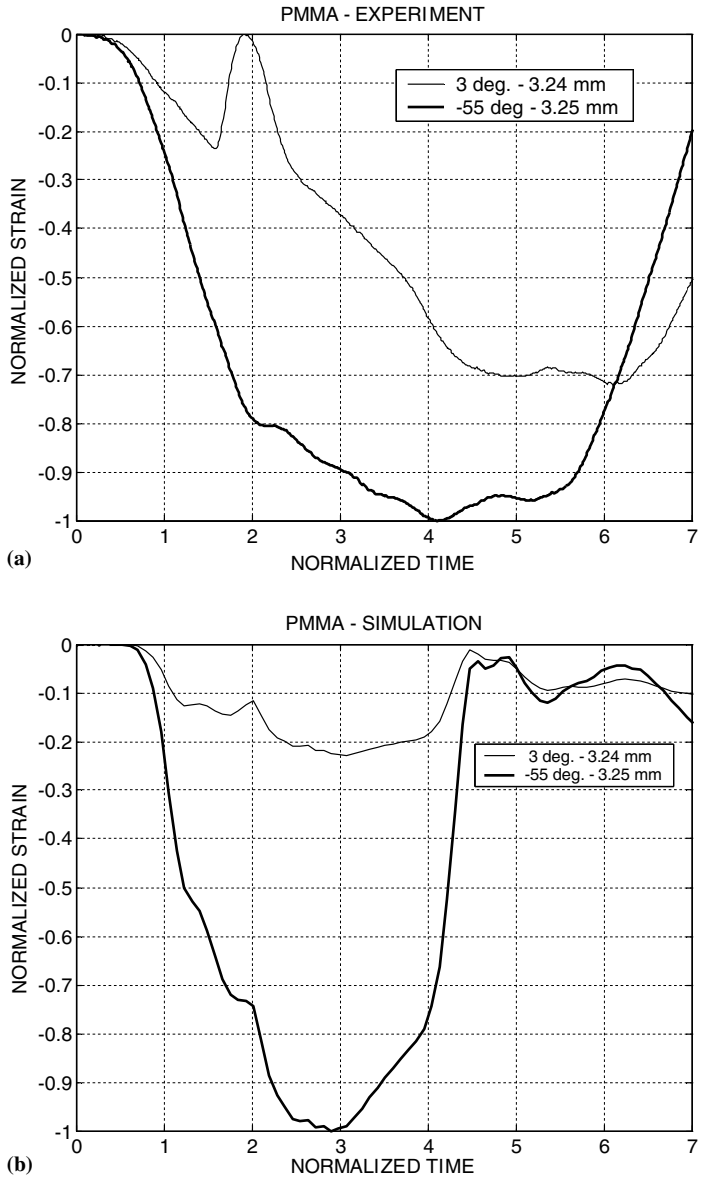

Fig. 6. PMMA experiment. Crack-tip strains: (a) measured and (b) calculated.

$E_N = 0.1Y$ and $E_N = 0.01Y$. The plane stress wave velocity is $c_d^{pl-\sigma} = 1450$ m/s, based on the above-mentioned mechanical properties of this material. Fig. 6(b) shows that the evolution of the two calculated strains is initially similar to that measured in the experiment. However, the parallel strain does not exhibit the observed drop. This discrepancy suggests that at $t \approx 1.5$, the specimen fractured so that the recorded strain signals related to crack propagation differ now markedly from the calculated strains. In this experiment, the absolute values of the SIF's at initiation are of little interest due to the multiplicity of cracks at failure.

This exercise illustrates nevertheless the applicability of the numerical tool to the detection of the onset of fracture.

4.2.2. Maraging steel specimen

In a typical experiment, the specimen was fatigue precracked, to obtain a 16.5 mm long crack. The specimen was loaded through a 12.7 mm diameter 250 Maraging steel bar. The side impact was applied by firing a 150 mm long striker at a velocity of the order of 45 m/s, as determined from a prior calibration. In the experiment described below, a noticeable shear band developed from the tip of the crack, as shown in Fig. 7 showing the crack region before and after impact. The strain gauges were cemented at $r_1 = 2.65$ mm—$\theta_1 = 1.4°$ (parallel), and $r_2 = 3.77$ mm—$\theta_2 = -74.7°$ (perpendicular), respectively. For the numerical calculation, a corresponding 63–3 μs risetime step pulse was modeled, and a "hard" contact configuration was assumed. The recorded and calculated strain gauge signals are shown in Fig. 8(a) and (b). The calculated strains have been normalized by the maximum absolute value of the strain. Note that the time origin of the experimental signals coincides with the origin of ε_{yy} while the time origin for the calculated strain corresponds to the onset of loading. A general similarity can be noted for the ε_{yy} component. By contrast, the experimental ε_{xx} component shows a slight initial negative phase (about 10 μs), followed by a marked positive phase which completely differs from the long negative phase of the calculated component. Fig. 8(c) and (d) shows the same gauge signals, both normalized in amplitude as a function of non-dimensional time. Here, the time origin of the two plots has been shifted to a common time at which the two ε_{yy} components decrease. From this figure, it appears clearly that the calculated and measured strains bear a high degree of similarity over a short normalized time period. The corresponding experimental and calculated stress intensity factors are calculated from Eq. (2), and they are plotted in Fig. 9(a) and (b), for the first 10 μs. This figure shows that the calculated K_{II} increases linearly for $t = 2$–5 μs, after which it gradually reaches a plateau. By contrast, the measured K_{II} increases almost linearly from 2 to 10 μs. A striking difference appears for the mode I component: whereas the calculated K_I is

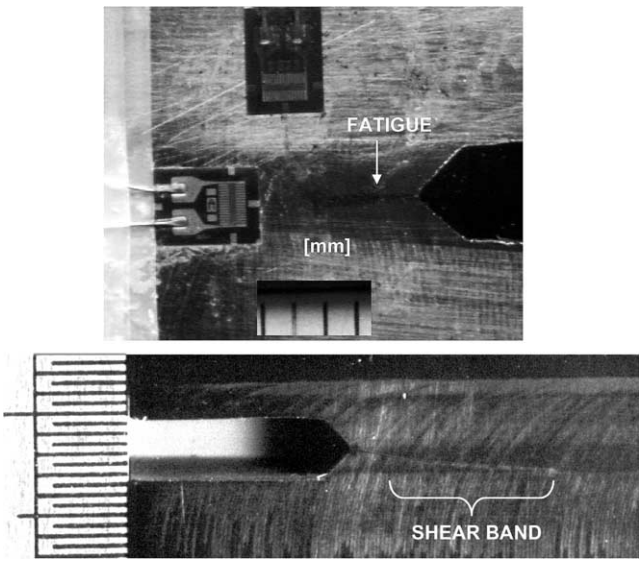

Fig. 7. Maraging 250 steel specimen, before and after impact. The fatigue precrack and strain gauges are shown before impact. Following impact, a long adiabatic shear band is clearly visible.

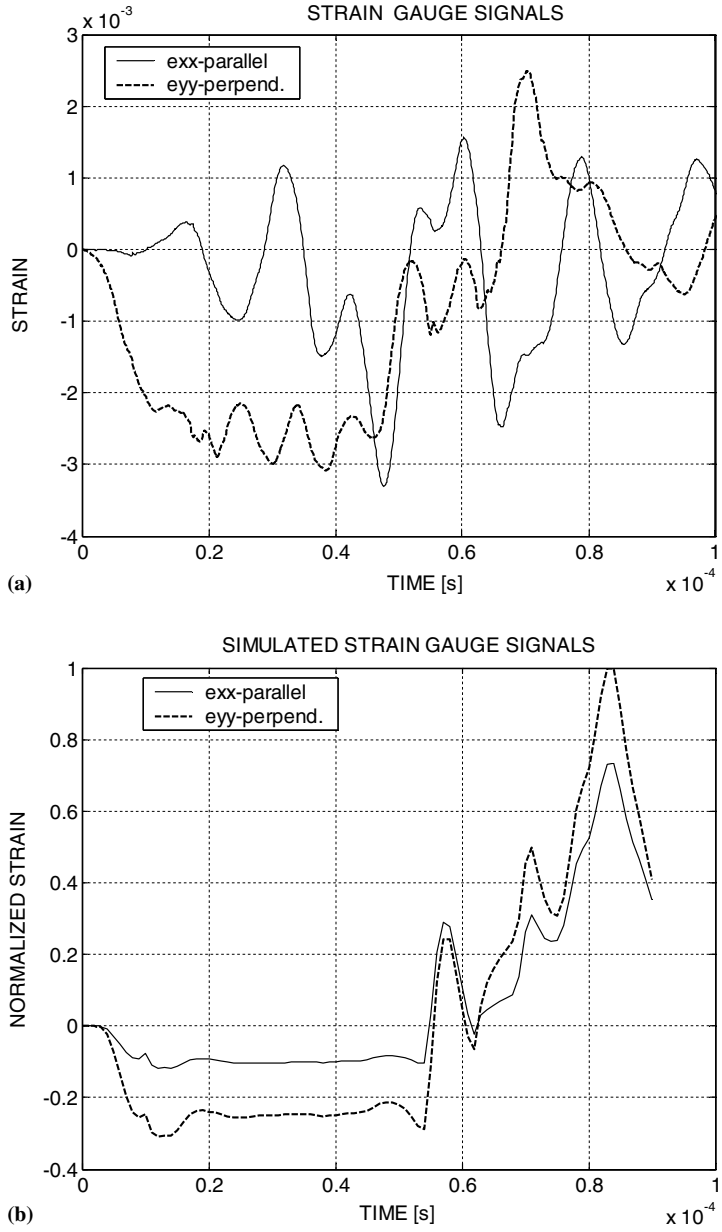

Fig. 8. Maraging 250 steel experiment. Crack-tip strains: (a) measured, (b) calculated, (c) and (d) are magnified initial parts of (a) and (b), respectively.

almost identically equal to zero over the considered time interval (after which it becomes negative as described previously—not shown in the figure), the measured K_I is positively increasing over the whole time interval. By drawing a tangent line to the calculated K_{II}, the end of the linear domain can be estimated to be $t^* \approx 4.6$ μs, at which the corresponding measured $K_{II} \approx 250$ MPa $\sqrt{\text{m}}$. This value is

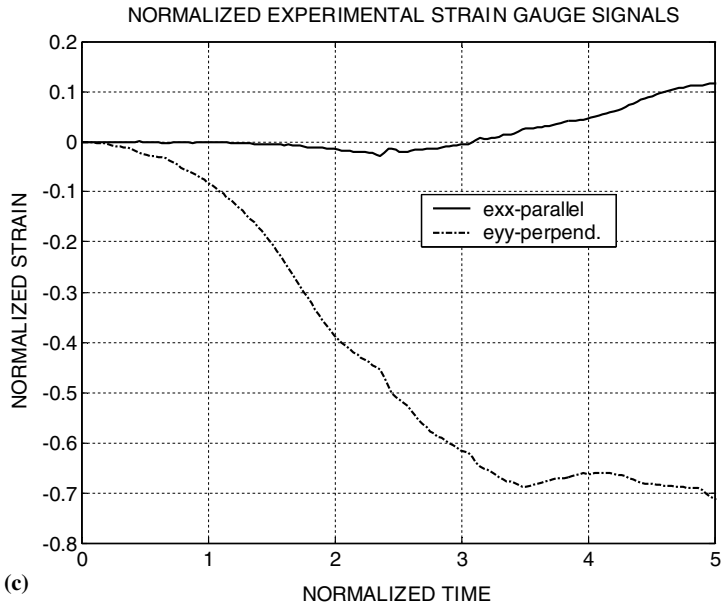

(c)

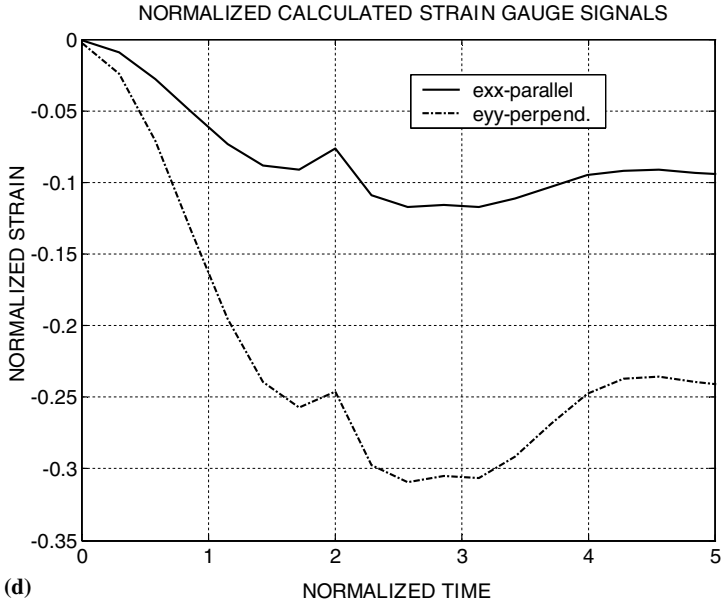

(d)

Fig. 8 (*continued*)

slightly higher than that reported by Guduru et al. [8] of $K_{II} \approx 130$–160 MPa $\sqrt{m}$, for this impact velocity. However, it agrees quite well with the value reported by Roessig and Mason [22] for 300 Maraging steel, $K_{II} \approx 220$ MPa $\sqrt{m}$. Besides toughness values, it should be noted that the divergence between numerical and experimental results has been successfully used to determine the conditions at which adiabatic shear banding develops.

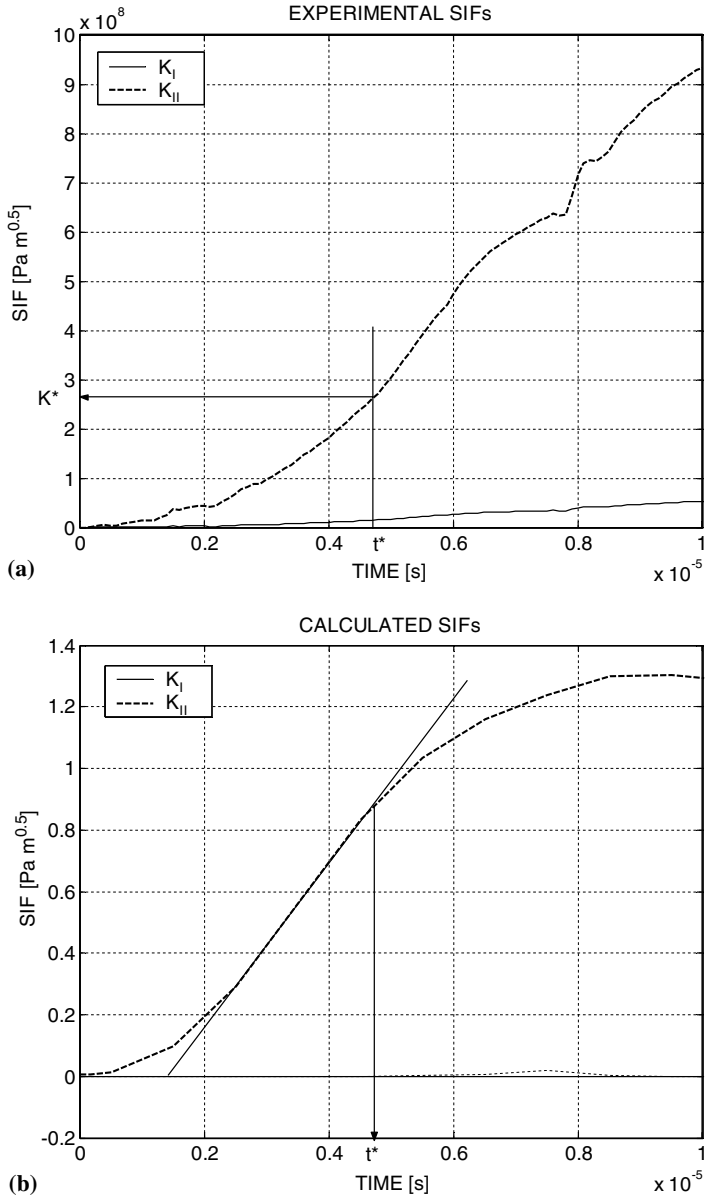

Fig. 9. Maraging 250 steel experiment. Stress intensity factors: (a) measured, (b) calculated. The experimental K_{II} is essentially linear for the whole duration, whereas the calculated K_{II} departs from linearity at $t^* \approx 4.6$ μs. At this time, $K_{II} \approx 250$ MPa $\sqrt{\text{m}}$.

5. Discussion

This work addresses the determination of the stress intensity factors for a stationary crack subjected to a dominant shear loading. While previous work has relied mostly on optical means to characterize the SIF's, the present work is based on the use of strain gauges to record transient signals at two arbitrary locations and determine the SIF's by solving a system of linear equations (Eq. (2)). As a general remark on the, it

should be noted that the central assumption is that the crack-tip fields are described by a single dominant parameter. This simplifying assumption is likely to induce some error in the accurate determination of the stress/strain field and a higher level of accuracy can be reached by introducing the higher order terms in Eq. (1). However, at this stage, it appears that a single parameter description of the crack-tip fields is reasonably accurate, as evidenced in the work of Weisbrod and Rittel [23]. The accurate position of the strain gauges is a delicate experimental problem. The determination of the radii and angles at which the strain gauges are cemented is based on measurements made on a photograph of the specimen. The experimental error in the radius is probably small, whereas the actual tilt of the strain gauge is more delicate to determine, and this is a potential source for experimental error [7]. It should be noted, on passing, that "stress intensity gauge" has been developed by Dally and Riley [5], and its reliability suffers from the same limitations of the present method, except that the exact angular and tilt of the strain gauge must be determined. Here, we assume that the gauge is not tilted with respect to the radius vector connecting it to the crack-tip, so that the actual ε_{xx} and ε_{yy} are measured.

As a final consideration, one wants to make sure that the strain gauges are cemented outside the plastic zone within the K dominated zone. Rice [18] provided an estimate of the plastic zone length, R, assuming a Dugdale strip subjected to pure mode II

$$R(t) = \frac{\pi}{8}\left(\frac{K_{\mathrm{II}}(t)}{\sigma_0}\right)^2 \tag{6}$$

For Maraging steel, a conservative estimate of the dynamic yield strength is $\sigma_0 = 2200$ MPa. Since the parallel gauge was cemented at $r = 2.65$ mm, the parallel strain can be reliably used for K_{II} values of up to 180 MPa $\sqrt{\mathrm{m}}$. Beyond this value, the parallel strain gauge reading ε_{xx} is probably influenced by plasticity in the shear band. Consequently, the measured shear banding toughness of $K_{\mathrm{II}} \approx 250$ MPa $\sqrt{\mathrm{m}}$ is probably overestimating the actual initiation toughness, which should therefore be $K_{\mathrm{II}} \approx 180$–$250$ MPa $\sqrt{\mathrm{m}}$, in close agreement with both Guduru et al.'s [8] results as well as those of Roessig and Mason [22].

The presented method relies on a simultaneous numerical simulation of the impact experiment and calculation of the SIF's and crack-tip strains. To keep the calculation to its simplest level, linear elastic assumptions are made. Yet, the contact problem induces two adjustable stiffnesses, which cannot be measured in a straightforward manner. Once the reliability of the numerical tool has been assessed, the comparison between experimental and simulated results provides a tool to interpret the experimental results.

Keeping these limitations in mind, a first assessment of the numerical tool was made by solving first Lee and Freund's [12] problem. A very good agreement was obtained for the short time interval during which the analytical solution is valid, including the slight crack closure, and this shows that the numerical tool provides reliable results. Next, additional validation was obtained by successfully simulating a real experiment carried out by Guduru et al. [8]. The central point of this exercise was to show that the deviation from the assumptions of linear elasticity and crack stationarity caused a divergence between the experimental results and their simulation. This divergence was used to identify a toughness value for adiabatic shear band formation.

Finally, experimental results were reported for a commercial brittle polymer (PMMA) and a high strength steel, similar to the material investigated by Kalthoff et al. [9] and by Guduru et al. [8]. The polymeric specimens fractured by producing three simultaneous cracks, so that the experimental and the numerical simulations could not be expected to be similar and were indeed dissimilar. On the contrary, the steel specimens failed by adiabatic shear banding. The strain gauge recordings could be compared with the calculated strains, and it was found that for a short initial time interval a high degree of similarity exists between the two. The comparison of the experimental and numerical simulation results indicated an initiation toughness $K_{\mathrm{II}} \approx 180$–$250$ MPa $\sqrt{\mathrm{m}}$, which is rather close to the value reported by Guduru et al. [8] of

$K_{II} \approx 130$–160 MPa $\sqrt{m}$. It should be noted that the comparison applies to different specimens, boundary and impact conditions, and method of assessment of the SIF's. Keeping in mind the potential sources of experimental error in the two methods, the present result shows the high potential for the hybrid experimental–numerical tool presented here, as a means of assessment of the transient SIF's.

The present method is quite simple to apply and relies on relatively simple experimental means. It can therefore be applied to a systematic investigation of the failure mode transition, aimed at, among other things, assessing whether the concept of a critical K_{II} can be reliably applied to the onset of adiabatic shear band formation.

6. Conclusions

The crack-tip fields which are characteristic of a dynamically loaded mode II crack have been investigated using a hybrid numerical–experimental approach, based on transient strain gauge recordings. The following conclusions can be drawn from the present study

- The numerical simulations can reliably reproduce the analytical results of Lee and Freund [12], and experimental results of Guduru et al. [8].
- As the calculations assume a stationary crack in a linear elastic material, a divergence between experimental and numerical results can be ascribed to the violation of the assumptions, i.e. crack propagation, large scale plasticity or adiabatic shear banding, as in the case of Guduru et al. [8].
- Our experiments with a brittle polymer and a high strength steel were analyzed using the proposed approach. The steel specimens developed adiabatic shear bands.
- For the case of steel specimens, the determined value of K_{II} at the onset of adiabatic shear banding was quite close to that reported by Guduru et al. [8], thus validating the overall approach through the cross-comparison of two different experiments and data reduction approaches.
- The proposed approach is quite simple and should easily be applied to the systematic study of the failure mode transition, including the assessment of a criterion for adiabatic shear band formation.

Acknowledgements

The author is indebted to Dr. R. Levin for her technical assistance, and to Mr. Y. Perelstein who participated to the experiments in the framework of a "Special Project in Mechanics" course. This research was partly supported by the Fund for Promotion of Research at Technion.

References

[1] ANSYS, User's manual, Ansys Inc., 2001.
[2] Barsoum RS. On the use of isoparametric finite elements in linear elastic fracture mechanics. Int J Numer Meth Engng 1978;10:25–37.
[3] Bathe KJ. Finite element procedures in engineering analysis. Englewood Cliff, NJ: Prentice-Hall; 1982.
[4] Bui HD, Maigre H, Rittel D. A new approach to the experimental determination of the dynamic stress intensity factor. Int J Solids Struct 1992;29(23):2881–95.
[5] Dally JW, Riley WF. Experimental stress analysis. New York: McGraw and Hill; 1991.
[6] Freund LB. Dynamic fracture mechanics. Cambridge: Cambridge University Press; 1990.
[7] Giovanola JH, Shockey DA. Dynamic fracture behavior of structural materials. SRI Intl Report #2777, Menlo Park, CA.
[8] Guduru PR, Rosakis AJ, Ravichandran G. Dynamic shear bands: an investigation using high speed optical and infrared diagnostics. Mech Mater 2001;33:371–402.
[9] Kalthoff JF. Shadow optical analysis of dynamic fracture. Opt Engng 1988;27:835–40.

[10] Kobayashi AS. Handbook on experimental mechanics. Englewood Cliffs, NJ: Prentice-Hall; 1987.
[11] Khanna SK, Shukla A. On the use of strain-gauges in dynamic fracture-mechanics. Engng Fract Mech 1995;51(6):933–48.
[12] Lee YJ, Freund LB. Fracture initiation due to asymmetric impact loading of an edge cracked plate. J Appl Mech 1990;57:104–11.
[13] Maigre H, Rittel D. Dynamic fracture detection using the force–displacement reciprocity: application to the compact compression specimen. Int J Fract 1996;73(1):67–79.
[14] Mason JJ, Lambros J, Rosakis AJ. The use of a coherent gradient sensor in dynamic mixed-mode fracture mechanics experiments. J Mech Phys Solids 1992;40(3):641–61.
[15] Mason JJ, Rosakis AJ, Ravichandran G. Full field measurement of the dynamic deformation field around a growing adiabatic shear band at the tip of a dynamically loaded crack or notch. J Mech Phys Solids 1994;42(11):1679–97.
[16] Ravi-Chandar K. On the failure mode transitions in polycarbonate under dynamic mixed mode loading. Int J Solids Struct 1995;32(6/7):925–38.
[17] Ricci V, Shukla A, Kavaturu M. Using strain gauges to investigate subsonic dynamic interfacial fracture in an isotropic–isotropic biomaterial. Engng Fract Mech 2003;70(10):1303–21.
[18] Rice JR. In: Fracture, vol. II. New York: Academic Press; 1968 [chapter 3].
[19] Rittel D. The influence of temperature on dynamic failure mode transition. Mech Mater 1998;30:217–27.
[20] Rittel D, Levin R. Mode-mixity and dynamic failure mode transitions in polycarbonate. Mech Mater 1998;30(3):197–216.
[21] Rittel D, Pineau A, Clisson J, Rota L. On testing of Charpy specimens using the one point bend impact technique. Exp Mech 2002;42(3):247–52.
[22] Roessig KM, Mason JJ. Adiabatic shear localization in the impact of edge-notched specimens. Exp Mech 1998;38(3):196–203.
[23] Weisbrod G, Rittel D. A method for dynamic fracture toughness testing using short beams. Int J Fract 2000;104:89–103.
[24] Zhou M, Rosakis AJ, Ravichandran G. Dynamically propagating shear bands in impact-loaded prenotched plates. I. Experimental investigations of temperature signatures and propagation speed. J Mech Phys Solids 1996;44(6):981–1006.
[25] Zhou M, Rosakis AJ, Ravichandran G. Dynamically propagating shear bands in impact-loaded prenotched plates. II. Numerical simulations. J Mech Phys Solids 1996;44(6):1007–32.